Journal of Histochemistry & Cytochemistry 2014, Vol. 62(6) 405–423
© The Author(s) 2014
Reprints and permissions:
sagepub.com/journalsPermissions.nav
DOI: 10.1369/0022155414531549
jhc.sagepub.com
SAGE

Characterizing and Diminishing Autofluorescence in Formalin-fixed Paraffin-embedded Human Respiratory Tissue

A. Sally Davis, Anke Richter, Steven Becker, Jenna E. Moyer, Aline Sandouk, Jeff Skinner, and Jeffery K. Taubenberger

Viral Pathogenesis and Evolution Section (ASD, JEM, AS, JKT); Bioimaging Section, Research Technology Branch (SB); and Laboratory of Immunogenetics (JS), Division of Intramural Research, National Institutes of Allergy and Infectious Diseases, National Institutes of Health, Bethesda, Maryland; Defense Resources Management Institute, School of International Graduate Studies, Naval Postgraduate School, Monterey, California (AR); Department of Population Health and Pathobiology, North Carolina State University College of Veterinary Medicine, Raleigh, North Carolina (ASD)

Summary

Tissue autofluorescence frequently hampers visualization of immunofluorescent markers in formalin-fixed paraffin-embedded respiratory tissues. We assessed nine treatments reported to have efficacy in reducing autofluorescence in other tissue types. The three most efficacious were Eriochrome black T, Sudan black B and sodium borohydride, as measured using white light laser confocal Λ^2 (multi-lambda) analysis. We also assessed the impact of steam antigen retrieval and serum application on human tracheal tissue autofluorescence. Functionally fitting this Λ^2 data to 2-dimensional Gaussian surfaces revealed that steam antigen retrieval and serum application contribute minimally to autofluorescence and that the three treatments are disparately efficacious. Together, these studies provide a set of guidelines for diminishing autofluorescence in formalin-fixed paraffin-embedded human respiratory tissue. Additionally, these characterization techniques are transferable to similar questions in other tissue types, as demonstrated on frozen human liver tissue and paraffin-embedded mouse lung tissue fixed in different fixatives. (J Histochem Cytochem 62:405–423, 2014)

Keywords

autofluorescence, formalin-fixation, paraffin-embedded tissue, immunohistochemistry, immunofluorescence, human, respiratory, confocal microscopy

Introduction

The successful visualization of fluorescent markers in formalin-fixed paraffin-embedded (FFPE) respiratory tissue sections is frequently hampered by tissue autofluorescence. Autofluorescence prevents the clean visualization of tissue-bound antibodies and lectins via immunofluorescence techniques, particularly when fluorochromes in the fluorescein isothiocyanate (FITC) range are used. The peak excitation of FITC is 500 nm and it emits at 75% relative intensity and greater from 506–532 nm (Life Technologies, Carlsbad, CA). Tissue autofluorescence has been attributed to many factors including endogenous tissue elements such as collagen, tissue processing techniques, particularly formalin fixation, and reagents such as serum that are applied to tissues during immunofluorescence protocols (Baschong et al. 2001; Billinton and Knight 2001; Collins 2006; Del Castillo et al. 1989). Key sources of autofluorescence in human tissue are likely lipofuscin, collagen, elastin, and red blood cells as well as formalin fixation (Banerjee et al. 1999;

Received for publication August 20, 2013; accepted March 3, 2014.

Corresponding Author:
Jeffery K. Taubenberger, Viral Pathogenesis and Evolution Section, National Institutes of Allergy and Infectious Diseases (NIAID), National Institutes of Health (NIH), 33 North Dr., MSC 3203, Bethesda, MD 20892, USA.
Email: taubenbergerj@niaid.nih.gov

10x Genomics EX2049
Bruker v. Harvard
IPR2024-00526

Baschong et al. 2001; Billinton and Knight 2001; Collins 2006; Monici 2005; Viegas et al. 2007). Additionally, endogenous flavins, reduced nicotinamide-adenine dinucleotide and nicotinamide-adenine dinucleotide phosphate are common causes of autofluorescence in cell cultures, where the brighter extracellular proteins are absent (Billinton and Knight 2001; Monici 2005; Viegas et al. 2007). Additionally, serum blocking has been suspected to increase autofluorescence (personal communication with staff at the Bioimaging Section, RTB, NIAID, NIH) and antigen retrieval techniques may also play a role (personal communication with multiple researchers at the NIH). The little evidence that has been reported has largely been observational data.

Because the vast majority of tissues for human and animal pathology over the last century has been treated with FFPE, this study focused on reducing autofluorescence in typical FFPE sections. Unless prospective tissue collection for a study is possible, alternative fixatives such as paraformaldehyde, which has been reported to decrease autofluorescence in tissues (Clancy and Cauller 1998), are not generally an option. Our selection of treatments for diminishing autofluorescence in FFPE human respiratory tissue was guided by methods reported in the literature and recommended by other immunofluorescence practitioners for a diverse collection of tissue types (Baschong et al. 2001; Beisker et al. 1987; Callis 2006; Clancy and Cauller 1998; Collins 2006; Cowen et al. 1985; Kittelberger et al. 1989; Schenk and Churukian 1974; Schnell et al. 1999). To our knowledge, there has been no published study focused on which of these reagents work best on FFPE respiratory tissues.

This study focused on characterizing and altering the autofluorescence profile of FFPE human tracheal tissue; specifically, the epithelium, lamina propria, and submucosa, as these tissue layers are of highest interest to respiratory pathologists and virologists. We measured and modeled autofluorescence overall as well as endogenous, element-specific autofluorescence in FFPE human tracheal tissue, tested techniques for diminishing and shifting this autofluorescence, and evaluated changes to the tissue autofluorescence profile that the most promising of these techniques produced. We characterized the autofluorescence signature for FFPE tracheal tissue by measuring overall tissue autofluorescence using the Λ^2 mapping technique on a Leica SP5 white light laser (WLL) confocal microscope and performing mathematical modeling; specifically, 2D Gaussian surface fitting. Finally, we assessed processes reported to increase autofluorescence as well as the most promising treatments reported to decrease autofluorescence using these same techniques.

Materials & Methods

Tissues

Anonymous donor human respiratory tissues, both lung and trachea, were obtained from Capital Biosciences (Rockville, MD). Briefly, tissues were harvested from human cadavers at no more than several hours post-mortem and fixed with 10% neutral-buffered formalin, dehydrated, and embedded in paraffin. Approximately 5-μm-thick sections were cut and placed on positively charged slides. Similarly sectioned slides of HistoChoice (Sigma-Aldrich, St. Louis, MO) and of formalin-fixed paraffin-embedded (FFPE) mouse lung tissue were provided by the NIH Clinical Center Critical Care Medicine Department and NIAID Viral Pathogenesis and Evolution Section, respectively. Frozen cirrhotic human liver tissue sections were provided by the NIAID Hepatic Pathogenesis Section.

Sample Preparation to Survey Techniques for Diminishing Autofluorescence

Sections of both human trachea and human lung tissue were used in this initial comparison of treatments reported to diminish autofluorescence. The nine treatments were as follows: trypan blue, Eriochrome black T, Sudan black B, Chicago (Pontamine) blue, sodium borohydride, tris glycine, ammonium chloride, ammonia ethanol and UV transillumination. The first four, which are dyes, were hypothesized to either shift or mask the autofluorescence emission profile. The latter five are quenchers, hypothesized to decrease the intensity of the autofluorescence without shifting its emission. One physical and four chemical quenching techniques were tested. With the exception of the UV transillumination and ammonia ethanol treatments (detailed separately in this section), all slides were rehydrated and antigen retrieved as previously described (Martinez-Anton et al. 2013). The treatment of interest was then applied, 1× TBSt with 0.02% Tween-20 washes were performed to remove the reagent at the end of the treatment, and slide was mounted in SlowFade Gold antifade reagent with DAPI (Molecular Probes; Carlsbad, CA). For all treatments, a volume sufficient to cover the tissue throughout the incubation time (approximately 200 μl) was applied.

For many treatments, titrations of the reagent as well as various incubation periods were tested iteratively until all failed or a satisfactory result was obtained. All treatment incubations were completed at room temperature. Trypan blue (250 μg/ml) in pH 4.4-adjusted 1× TBS was applied for 1 min (Collins 2006; Schenk and Churukian 1974). Eriochrome black T (EBT; 1.65%) was dissolved in DI water and applied for 5 min, as per personal communications with Robert Cunningham (formerly of the Armed Forces Institute of Pathology) (Kittelberger et al. 1989; Schenk and Churukian 1974). Sudan black B (SB) was prepared as 0.3% in 70% ethanol stirred in the dark for 2 hr and then applied to tissues for 10 min (Baschong et al. 2001; Collins 2006; Schnell et al. 1999). To achieve the necessary staining translucency for bright field microscopy of the tissue, SB slides were rinsed briefly in 70% ethanol (EtOH)

Table 1. Treatment Abbreviations in their Order of Introduction.

Abbreviation	Treatment
No antigen retrieval and no serum	No AR No Se
No antigen retrieval and serum	No AR Se
Antigen retrieval and serum	AR Se
Antigen retrieval and no serum	AR No Se
Eriochrome black T, no antigen retrieval and no serum	EBT No AR No Se
Eriochrome black T, No antigen retrieval and serum	EBT No AR Se
Eriochrome black T, antigen retrieval antigen retrieval and serum	EBT AR Se
Eriochrome black T, antigen retrieval and no serum	EBT AR No Se
Sodium borohydride, antigen retrieval and serum	NB AR Se
Sodium borohydride, no antigen retrieval and no serum	NB No AR No Se
Sudan black B, antigen retrieval and serum	SB AR Se
Sodium borohydride, Eriochrome black T, antigen retrieval and serum	NB EBT AR Se
Sodium borohydride, Sudan black B, antigen retrieval and serum	NB SB AR Se

followed by additional washing. Chicago blue was prepared at 0.5% in 1× TBS and then applied to tissues for 10 min (Collins 2006; Cowen et al. 1985). Sodium borohydride (NB) was prepared at 1 mg/ml in 1× TBS and kept on ice. It was applied to tissues for three consecutive 10 min incubations without any intermediary washes (Baschong et al. 2001; Beisker et al. 1987; Clancy and Cauller 1998; Collins 2006). Tris-glycine was prepared from 0.1 M glycine in TBS, adjusted to pH 7.4 using Tris, and applied to slides for 30 min (Callis 2006; Collins 2006). Ammonium chloride (50 mM) in 1× TBS was applied to tissues for 10 min (Callis 2006). After rehydration in 70% EtOH, a solution of 70% EtOH with 0.5% ammonia was applied for 1 hr, and then rehydration was resumed with the addition of a 50% EtOH step followed by distilled water. Slides then underwent antigen retrieval and finally were washed in 1× TBS and mounted as described for the other treatments (Baschong et al. 2001). UV treatment consisted of either 8- or 24-hr transillumination of the dehydrated tissue on a UVB transilluminator (Ultra Lum, Inc.; Claremont, CA), with a range between 280–320 nm. The tissues were covered with foil prior to rehydrating and mounting as per above (Neumann and Gabel 2002). Slides were reviewed and compared with an untreated slide using a Leica SP5 WLL confocal system (Leica Microsystems, Wetzlar, Germany).

Sample Preparation for Analysis of Baseline Autofluorescence

In the following analyses, all human trachea slides were serially sectioned from the same FFPE tissue block so that variation in tissue fixation and processing was held constant across treatment comparisons. In order to rule out the possibility that antigen retrieval or serum application increased tissue autofluorescence and to establish a picture of baseline autofluorescence in human tracheal tissue, the following human tracheal tissue slides were evaluated: no antigen retrieval (AR) without serum (No AR No Se), no AR with serum (No AR Se), AR with serum (AR Se), AR without serum (AR No Se). All treatment abbreviations used in the human tracheal tissue portion of this study are listed in Table 1. Regardless of treatment, all slides were rehydrated as per above. Slides that received AR and/or serum were processed as described followed by a 5 min 1× TBSt wash with several fluid exchanges in order to simulate washes that would occur during typical immunofluorescence protocols. Slides were maintained in 1× TBSt between treatments. Slides were mounted in ProLong Gold Antifade Reagent (Molecular Probes) as per vendor's instructions. This change from SlowFade Gold with DAPI to Prolong Gold was deliberate, as the latter enables longer-term preservation of fluorescence. Additionally, samples were not stained with DAPI so that autofluorescence spectra could be collected with 405 nm excitation.

Sample Preparation to Measure Effect of a Select Number of Treatments

In order to examine the possibility that AR and serum application might interact with a downstream treatment, AR and serum application were continued in conjunction with the next two treatments, EBT and NB, which are targeted at diminishing autofluorescence.

We applied EBT treatment to human tracheal sections in conjunction with AR and serum, which resulted in four combinations of treatments (see Table 1). The same procedure as detailed in the last section was followed for this slide production with the addition of the application of freshly prepared 1.65% EBT for 5 min after the serum application stage. Slides were then mounted in ProLong Gold. NB treatment was analyzed with the following

combinations: NB AR with serum (NB AR Se) and NB No AR without serum (NB No AR No Se). We also looked at the effect of SB in conjunction with AR and serum (SB AR Se) to compare with EBT AR Se. Additionally, some combination treatments were explored, including NB with EBT (NB EBT AR Se) and NB with SB (NB SB AR Se) both with AR and serum. In the above preparations, serum was applied after NB whilst serum was applied before EBT and SB, as per previous recommendations (Baschong et al. 2001; Clancy and Cauller 1998; Kittelberger et al. 1989; Schenk and Churukian 1974; Schnell et al. 1999). Finally, in order to separate tissue-dependent results from treatment-dependent results, serial and/or step sections of AR Se, EBT AR Se, NB AR Se and SB AR Se were made.

Data Capture on the Leica SP5 White Light Laser Confocal System

Three fields, each always including regions of epithelium, lamina propria and submucosa, were analyzed for each of the 13 treatment combinations listed in Table 1. An additional experiment on triplicate sections with four of the treatments—AR Se, EBT AR Se, NB AR Se and SB AR Se—was also conducted in order to account for tissue section-dependent changes in the results. Data were collected with a 40×, 1.25 NA oil immersion objective at 600 Hz, bidirectional capture, 512×512 pixels, 387.50×387.50 μm field-of-view, pinhole 1 AU without any averaging or accumulation.

The WLL pump power was set at 60% directly on the laser unit. This compensation was done so that the measurements for the peak intensity of autofluorescence for all treatments fell within the range of the initial data and consequently was amenable to mathematical modeling. For more information on the WLL pump power, please see the Supplemental Methods.

Λ^2 WLL data was gathered in the xyλΛ acquisition mode (Leica Microsystems 2010), with the following excitation/emission scan settings: excitation range 470–670 nm, Λ-excitation step size 5 nm, detection range 480–780 nm, detection bandwidth 10 nm, and λ-detection step size 10 nm. During all sessions, the smart gain was 1020.8 and the smart offset -3.4%. Accompanying fluorescent images were collected for each data point. Post-data acquisition, excitation/emission scan contour plots and 3D views were produced in LAS AF Software (Leica Microsystems) for the Λ^2 data; this data was then exported for further processing in Origin Lab Pro version 9.0 (OLP) (OriginLab Corporation; Northhampton, MA) and Microsoft Excel (Microsoft Corp.; Redmond, WA).

Emission data at 405 nm and 458 nm were gathered using the UV diode and Argon lasers at 11% and 18%, respectively, and the xyλ acquisition mode. For the 405 nm excitation, the following λ-scan range properties were employed: detection range, 415-775 nm; detection bandwidth, 10 nm; and detection step size, 10 nm. The 458 nm λ-scan settings were detection range, 470-770 nm; bandwidth, 10 nm; and step size, 10 nm. The 405 and 485 nm lambda data were also reviewed in LAS AF using the Quantify functionality and then exported for further analysis in Excel.

Images demonstrating autofluorescence levels in the green wavelengths and their change due to treatments were taken with a 40× oil objective, NA of 1.25 using the following settings on the WLL: pinhole, 1 AU; 387.50×387.50 μm field-of-view; 1024×1024 pixel format; line averaging, 4; HyD gain of 100%;. An additional set of images demonstrating representative autofluorescence for AR Se, No AR Se, No AR No Se, and AR No Se were taken on a Leica SP8 confocal system with the following settings: pinhole, 1 AU, 387.50×387.50 μm field-of-view; 1024×1024 pixel format; line averaging, 4; HyD gain of 100%, with a 40× oil objective, NA of 1.25. For a given panel, the images were taken during a single session on serial sections of the same tracheal tissue. This was done in a separate session from the Λ^2 data capture because the images taken during those sessions are only 512×512 pixels. However, all Λ^2 session images and intensity data are provided in the form of image arrays produced in OLP from the LAS AF data.

Mathematical Modeling of Λ^2 Data

Data captured on WLL was imported into OLP. It was fit to a functional form using the Data Fitting command. Different functional form fits were compared using the Compare Models command, which calculates the Akaike's Information Criterion (AIC) test. Functional forms that we considered were 2-dimensional (2D) Gauss, 2D LogNormal, 2D Voigt, 2D Lorentz, 2D Rational and 2D Gaussian. According to the AIC test, the Gaussian provided the best fit for the baseline data (AR Se, AR no Se, No AR Se, and No AR No Se) when compared against each of the other functional forms. This function form (2D Gaussian) was then maintained for the other treatments to permit cross treatment comparisons, even though certain treatments did have features that would have lent themselves to more complex functional forms with multiple peaks. Data reports for the model fits are provided as TIFF files exported from OLP. The 2D Gaussian function has seven parameters, but the four that were felt to be most biologically relevant were the location of the central peak of emission intensity (x_c, y_c) and the overall intensity of the emission, which was calculated from the floor of the functional form (z_0) and the peak intensity from this floor (A). Because fitting a 2D functional form is an estimation procedure that is a far more complex algorithm than with a typical 1D form, with slightly more or slightly less data it is possible to obtain a different model fit or for the fitting algorithm not to converge. To determine

the variations of model fit possible with the given data, two models at a minimum were fit for each data set collected. The models were created by progressively eliminating the low intensity levels, wherein the greatest noise was observed. For example, the first model would be fit using all of the available data; the second model would be fit using only data with an intensity greater than 1; and the third model would be fit only using data with an intensity greater than 2. If a model failed to converge, the next level of intensity would be eliminated and the model would be fit again. Because of this fitting procedure, the floor of the model (z_0) would rise by necessity and hence, to obtain emission intensity levels, it is necessary to add this floor to the peak emission. As, for each treatment, three fields of data were captured, a total of at least six model fits were made per treatment. For each of these fits, the four model fit parameters were exported to Excel for further analysis. Additionally, graphics were created in OLP using both the raw data and the fitted models (as detailed in the next section).

Examination of Fixed Mouse Lung Tissue Autofluorescence

In another set of experiments, we compared otherwise untreated mouse lung tissue fixed with HistoChoice (Sigma-Aldrich; St Louis, MO) with mouse lung tissue fixed with 10% neutral-buffered formalin. We used the Λ^2 data collection techniques detailed above and then analyzed the resulting raw 3D data in OLP.

Effect of Eriochrome Black T and Sudan Black B on Frozen Human Liver Tissue

Experiments with cirrhotic human frozen liver tissue sections were used to examine the effect of EBT and SB on this tissue type. Three slides were prepared: untreated, EBT and SB. Frozen tissue slides were incubated in 100% ethanol for 10 min at -20C. Without waiting for them to dry, they were rehydrated by washing in PBS with 0.01% Tween-20 (PBSt) twice for 5 min each. The slides were then blocked for 20 min with 10% normal goat serum diluted in PBSt, washed in PBSt for 20 min, followed by two washes in PBS only. EBT or SB was applied as per the earlier described methods or the slide was left in PBS. Finally, slides were mounted in ProLong Gold. Similar to the mouse tissue analysis above, we used the Λ^2 data techniques to analyze the effect of the EBT and SB on this tissue type.

Data Analysis

Once the Λ^2 model data was imported into OLP the mean, standard deviation, and standard error emission intensity level were calculated for each treatment and plotted in a boxplot. In addition, scatter plots were created to permit comparison of the locations of the central peak of emission intensity (x_c, y_c) for each model fit for each treatment. Smaller intensity levels equated to less autofluorescence with a value of zero representing an absence of autofluorescence detection at a given excitation/emission pairing. Relative emission intensity is unitless, but for presentation it is scaled and expressed using an 8-bit scale (0–255). Emission intensity is a function of both laser power and efficiency of excitation. The WLL output is not constant across all wavelengths. In order for the sample to be excited by constant power at each wavelength, the output of the laser is automatically adjusted. Therefore, the relative emission across the spectrum can be compared.

3D surface plots of raw WLL Λ^2 data as well as model output virtual matrices were created in OLP using Open GL 3D Surface Plot functionality. They enabled visual comparison of raw to modeled data for individual treatments, inter-field comparison for a single treatment and comparison of treatments in the form of 3D surfaces. Specifically, hybrid graphs composed of multiple color fill and matrix scatter surfaces were used to improve visual discrimination of this data. The choice of color fill vs. matrix scatter has no other significance with the exception of graphs that display raw data vs. model output, for which the former is a color fill surface and the latter a matrix scatter surface.

Data at 405 nm and 458 nm xyλ were directly imported into OLP for all analyses. Emission data for each excitation was graphed for three fields for each treatment slide and visually examined for differences in the shape of the emission intensity spectrum. The x and y-axes for these graphs were standardized within each laser excitation group. Because the 405 nm and 458 nm data were generated through the use of two different lasers, their intensity values were not comparable to each other. In addition, the maximum emission intensity was calculated for each field and the mean, standard deviation, and standard error for the maximum emission intensity was calculated for each treatment. Boxplots permit comparison of this data. Finally, the y-axes for the 405 nm, 458 nm and WLL intensity plots have different ranges on their y-axes. These are reflective of individual laser-dependent intensity ranges, which are also non-comparable between data sets.

In addition to the aforementioned summary statistics, we produced scatter plots of the locations of the central peak of emission intensity (x_c, y_c) for each model fit of each treatment in Excel. We attempted to compare the locations of the central peaks using AIC comparisons, extra sums of squares F-tests, and multiple analysis of variance (MANOVA), but none of the results were satisfactory. Therefore, graphical assessment of the actual data was used instead to make comparisons among the different treatment options. For more details, see the Supplemental Section.

Table 2. Comparison of Treatments for Diminishing Green Wavelength Autofluorescence in Human Respiratory Tissue.

Treatment	Reduction in Autofluorescence	Interference with Other Channels	Ease of Preparation and Reproducibility
Trypan blue	0	3	3
Eriochrome black T	3	1 (faint black residue visible on bright field, rhodamine red autofluorescence increased, DAPI visibility decreased)	3
Sudan black B	3	0 (black residue obvious, bright field clarity poor, DAPI visibility decreased, boils under MP)	0
Chicago (Pontamine) blue	2	2 (DAPI visibility decreased)	3
Sodium borohydride	3	3	2
Tris glycine	1	3	2
Ammonium chloride	0	3	2
Ammonia ethanol	2	3	3
UVB transillumination	1	3	2

This summary of findings for the survey of techniques for diminishing FITC channel autofluorescence reveals variability in the reduction of this autofluorescence from 0 (no visible effect) to 3 (marked reduction); the degree of interference with other channels, including bright field visualization, DAPI, and rhodamine red visualization, and MP excitation from 0 (marked interference) to 3 (no interference perceived), with the descriptor characterizing the interference; and variability in ease of preparation and reproducibility of the technique over multiple protocol runs from 0 (complex to prepare and hard to reproduce a consistent result) to 3 (easy to prepare and highly reproducible).

Intensities were compared among the 13 treatment groups (Table 1) using one-way ANOVA with Tukey post-hoc tests for multiple comparisons. This analysis was done in JMP 10.0.0 64-bit edition (SAS Institute; Cary, NC). As this is a comparison of all possible treatment pairs, we present the results in the form of a connected letters report (in Tables 3, 4, and 5), which shows the mean (average) maximum intensity for each treatment as well as the groupings into which each of the treatments were categorized. Treatments not sharing a letter are significantly different from each other; treatments sharing a letter are not significantly different.

Confocal images presented in figure panels were post-processed in Imaris 7.6.3 (Bitplane; Zurich, Switzerland). However, Λ^2 session images, which were exported in TIFF format from the Leica software and uploaded directly into OLP for image array assembly, were not post-processed in Imaris.

Results

Three Treatments Significantly Diminish Green Wavelength Autofluorescence

Nine treatments, previously reported to reduce autofluorescence in a diverse range of cells and tissue types, were semi-quantitatively graded for their ability to reduce autofluorescence in FFPE human respiratory tissue. These treatments were also assessed for their level of interference with visualization on other channels such as DAPI (75% intensity emission range 431–492 nm) and rhodamine red (75% intensity emission range 582–602 nm) (Life Technologies), as well as ease of preparation and reproducibility of the treatment (Table 2). A 0–3 scale was used to grade the reduction in autofluorescence, from no appreciable reduction (0) to marked reduction (3); to describe degree of interference with other channels including bright field visualization, from marked interference (0) to no interference perceived (3); and to present the ease of preparation and reproducibility of the treatment, from time consuming or complex to prepare, with high variability in treatment effect (0) to easy to prepare and a readily repeatable effect on autofluorescence (3).

EBT diminished tissue autofluorescence in the green wavelengths (Fig. 1A, 1B). However, it shifted (i.e., moved the highest intensity components of) this autofluorescence from the green to red wavelengths. NB was the most effective quencher, diminishing yet not shifting the autofluorescence (Fig. 1C). SB, although more labor intensive in its preparation and its application, also showed promise (Fig. 1D). It appeared to mask the autofluorescence rather than shifting it. UV treatment showed minimal change, likely because the range of UV exposures did not adequately overlap with that of the tissue autofluorescence. The other quenchers and dyes either failed entirely, despite titrations of concentration and extensions of incubation time, or had only minimal effect, markedly less than the three aforementioned treatments.

EBT, NB and SB, the most promising treatments for diminishing autofluorescence on human respiratory tissue, were thus selected for further study. We also added steam antigen retrieval and serum application to our study set because both are frequently used in immunofluorescence protocols and concerns had been raised regarding each of

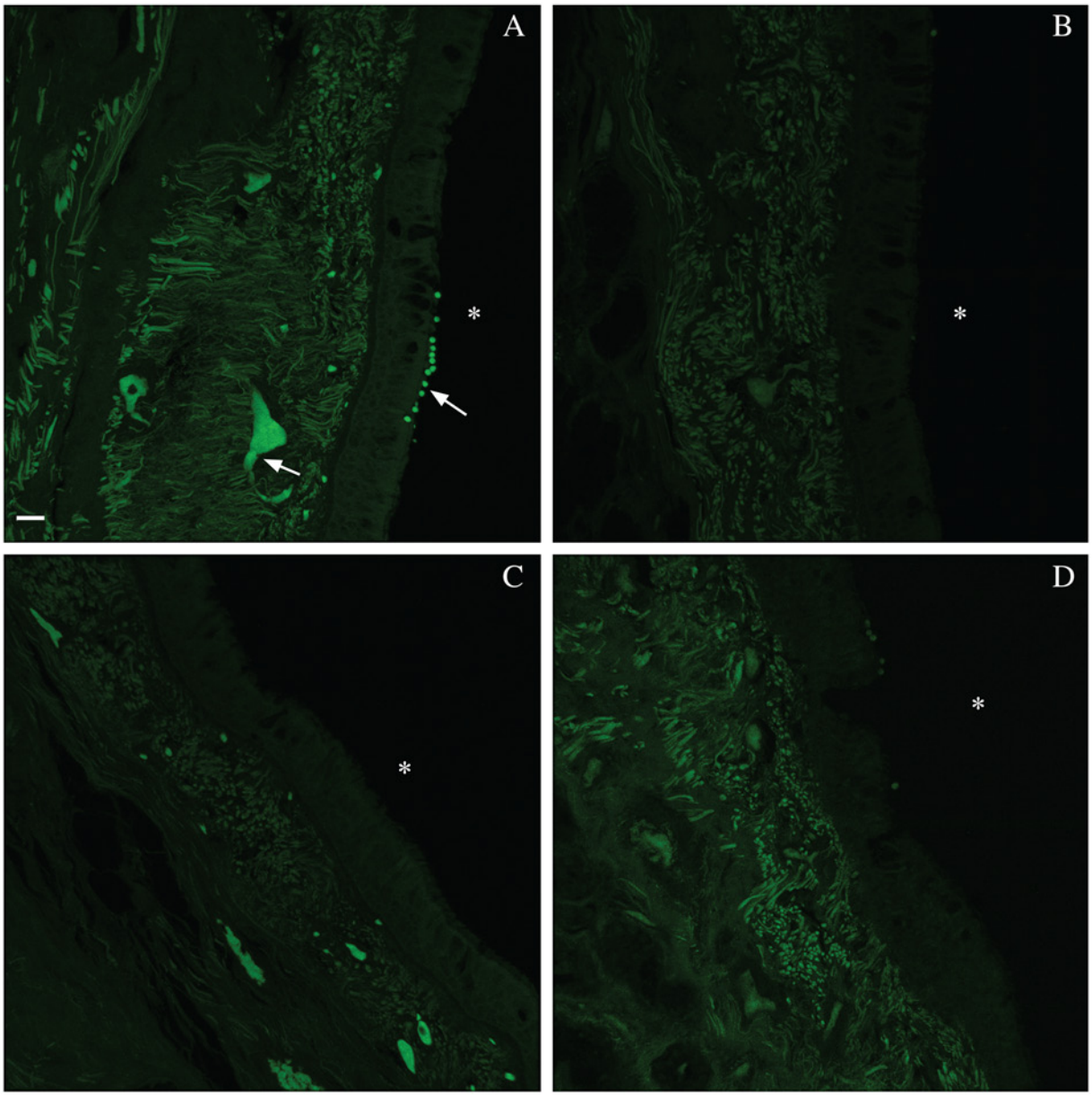

Figure 1. Reduction of autofluorescence in formalin-fixed, paraffin-embedded (FFPE) human tracheal tissue by three treatments. Comparison of green wavelength autofluorescence (AF) in tracheal FFPE tissue slides that received antigen retrieval and serum application +/- AF diminishing treatment: (A) untreated control, (B) Eriochrome black T, (C) sodium borohydride and (D) Sudan black B. Images were taken on a Leica SP5 WLL confocal system and are presented as maximum projections of 11.33-µm-sized z-stacks; excitation was with an Argon laser (488 nm) at 4% and detection range was 504–553 nm. White asterisks denote the tracheal lumens. Arrows denote red blood cells within vessels and extravasated red blood cells. Bar: 20 µm.

them contributing to an increase in autofluorescence. The full set of treatments for this section of the study and their acronyms is listed in Table 1. Finally, because the differences between autofluorescence level change on lung and tracheal tissue were minimal, the tissues to be tested were narrowed to human tracheal tissue for the remainder of the study.

Mathematical Modeling of Λ^2 Data is a Valid Technique for Comparing Treatment Effects

In order to compare treatment-induced changes in human tracheal tissue autofluorescence, we captured autofluorescence intensity images using Leica Λ^2-technology on the

Leica SP5 WLL confocal system (Leica Microsystems 2010). For each excitation, a full series of emission measurements was made for the entire field. A 2D intensity map and corresponding image was constructed for each excitation/emission combination so that all the intensity data could be reviewed in a single 3D surface graph. With this approach, for each pixel, the full photonic range was captured, not just the peak intensity. Given our data collection settings (as described in the Materials & Methods), for each field analyzed, we generated 769 images of autofluorescence with all possible excitation/emission combinations. We provide these images paired with their intensity values in image arrays, one per field measured (Supplemental Fig. S2A–2NN). In order to compare these data in a more quantitative fashion than direct visual inspection of individual images or via the 3D surface generated for each field, we fitted the data to 2D Gaussian surfaces and focused on model outputs with biological significance. All model fit reports are provided as supplemental data (Supplemental file: "Model Fits.docx"). The model fit outputs of biological significance were central peak of emission intensity (x_c, y_c) and the overall intensity of the emission, which was calculated from the floor of the functional form (z_0) and the peak intensity from this floor (A). The overall process of data collection and analysis for a single field on one treatment slide is summarized in Figure 2 (and in Supplemental Fig. S8).

The raw Λ^2 data for both AR Se fields and EBT AR Se fields fit the 2D Gaussian model (Fig. 3A, 3B; Supplemental Fig. S3A–S3D), and the model fit similarly across raw data sets within a treatment (Fig. 3C, 3D). This demonstrated that the model fit the most disparate treatments reasonably well (i.e., no treatment and EBT). We, therefore, compared treatment results at the model level instead of at the raw data level.

In order to determine if inter-slide variation would necessitate the use of multiple tissue sections per treatment, we compared multiple slides (non-serial sections) from the same tissue block for a sub-set of treatments: AR Se, EBT AR Se, NB AR Se and SB AR Se. We found that the intra-slide field variation was, at times, greater than the inter-slide field variation. Therefore, we considered a single tissue section heterogeneous enough to represent autofluorescence ranges expected for a given treatment on multiple sections cut from the same tissue block.

Steam Antigen Retrieval and Serum Application Have Minimal Effect on Tissue Autofluorescence

As we suspected from our visual review of images, modeling and analysis revealed that AR and Se application did not impact the autofluorescence signature on otherwise untreated tissues across the channels analyzed: 470–670 nm WLL, 458 nm and 405 nm excitations. Representative green wavelength tissue autofluorescence images for these four treatments are shown in Supplemental Figure S4A–S4D. 3D surface plots of representative model fits of the Λ^2 data for each of the four treatments—AR Se, No AR No Se, AR No Se and No AR Se— showed minimal variation in model fit (Fig. 4A). A scatterplot of x_c vs. y_c revealed that the central peaks of emission intensity were tightly grouped and overlapping for all four treatments; two model fits for all three fields from each treatment are shown (Fig. 4B). A box plot of intensity levels (sums of z_0 and A) also showed overlap for these four treatments (Fig. 4C) consistent with the ANOVA results showing no statistical difference (Table 3). The increased intensity in the serum application surfaces seen in the representative model comparison (Fig. 4A) averaged out to no difference across all data sets (Fig. 4C; Supplementary Fig. S5A–S5D) and was therefore not significant (Table 3). Additionally, there was little variance in the central peak of the autofluorescence emission and intensity levels at 458 nm and 405 nm excitations (Fig. 5A–5D and Tables 4, 5).

Eriochrome Black T Shifts Tissue Autofluorescence with Antigen Retrieval Only

We found the role of AR to be critical when using EBT but that serum application made no appreciable difference. 3D surface plots of representative model fits of the Λ^2 data for each of the four EBT treatments—EBT AR Se, EBT No AR No Se, EBT AR No Se, and EBT No AR Se—showed that only EBT AR Se and EBT AR No Se applications resulted in a striking right shift (increase in wavelength) of the central peak of intensity (Fig. 6A). This finding was also seen in a scatterplot of the central peaks of emission intensity where EBT treatment with AR groups separated from EBT treatments without AR (Fig. 6B). The WLL intensity box plot shows that the average intensity levels of the EBT AR-treated slides were twice that of the EBT non-AR slides, and that the EBT non-AR treatments were equivalent to the non-EBT AR treatments discussed earlier (Fig. 4C and Table 3). A comparison of EBT AR Se to AR Se revealed a right shift in autofluorescence wherein tissue autofluorescence was markedly decreased in the green wavelengths emission range but increased in the red wavelengths emission range (Fig. 6C) and the scatterplot of AR treatments with and without EBT showed distinct groupings of the EBT AR slides and non-EBT AR slides (Fig. 6D). The 458 nm and 405 nm excitations intensity boxplot data for the four EBT treatments showed no statistical differences in mean intensity levels between these treatments (Fig. 5C, 5D and Tables 4, 5). However, review of the full emission profiles for both of these revealed a partial shift in autofluorescence in all slides treated with EBT and AR (Fig. 7A, 7B)

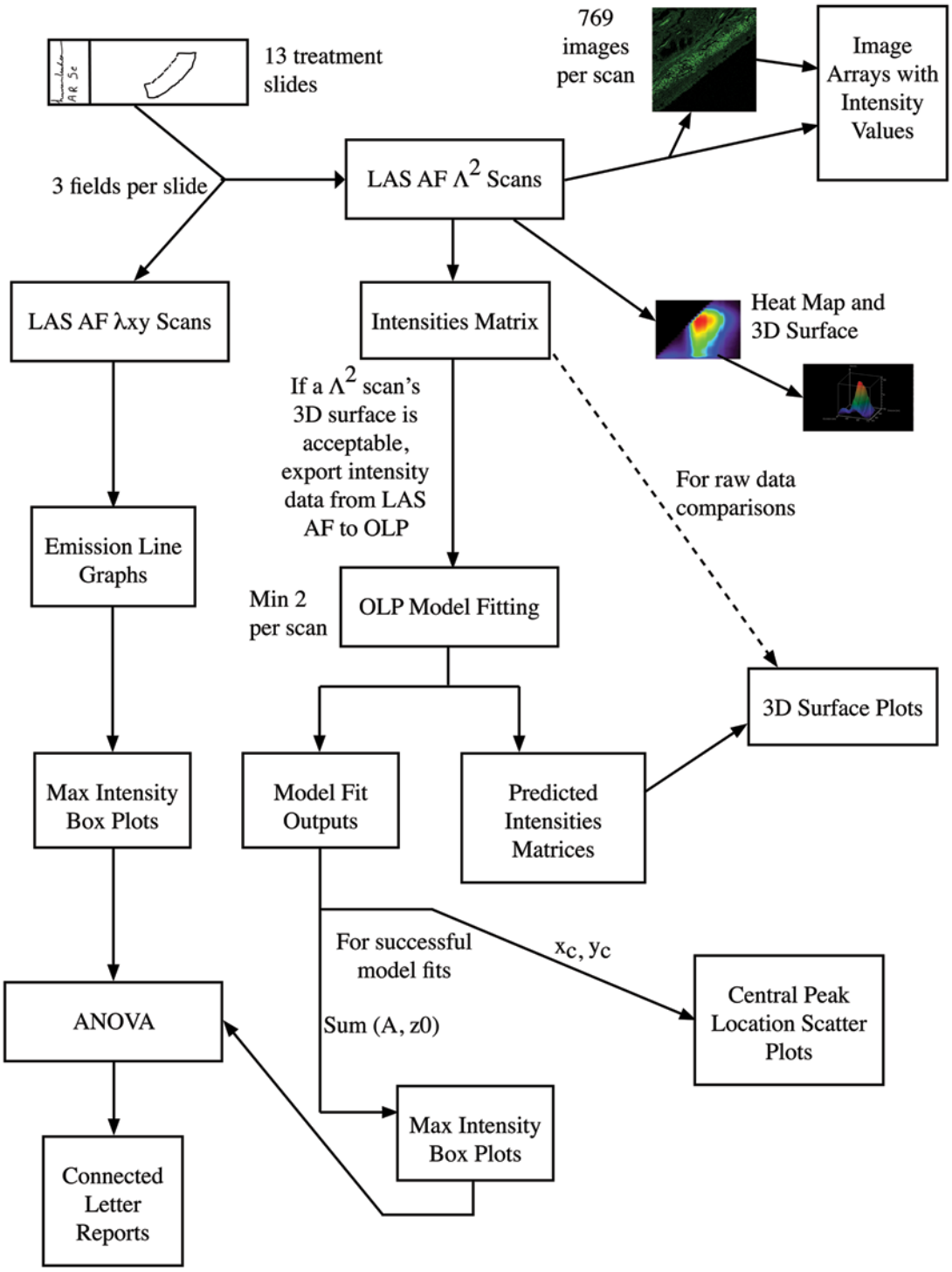

Figure 2. Λ^2 data collection and analysis process flow diagram. The flow chart depicts the entire analysis process that was followed in this research. The process starts in the upper left hand corner with the creation of the treatment slides. Following the arrows leads to two different scanning processes that were used to analyze the slides. For each of the scanning processes, different assessments and evaluation techniques were employed. One scanning process created 2-dimensional data which was analyzed with line graphs and box plots of the maximum intensities. The other scanning process created 3-dimensional (3D) data. The scanning software itself produces several images and output arrays (the two right-most arrows out of "LAS AF Λ^2 scans") and the data were also analyzed by mathematical software that allowed us to fit surfaces to the data to permit the comparison of the different treatments. This allowed us to create 3D surface plots as well as assess and compare the location of the central peak and the relative intensity observed at this peak for each of the treatments. ANOVA analysis was used to compare the maximum intensities between treatments to determine if there were any significant differences. This is summarized in the connected letters reports.

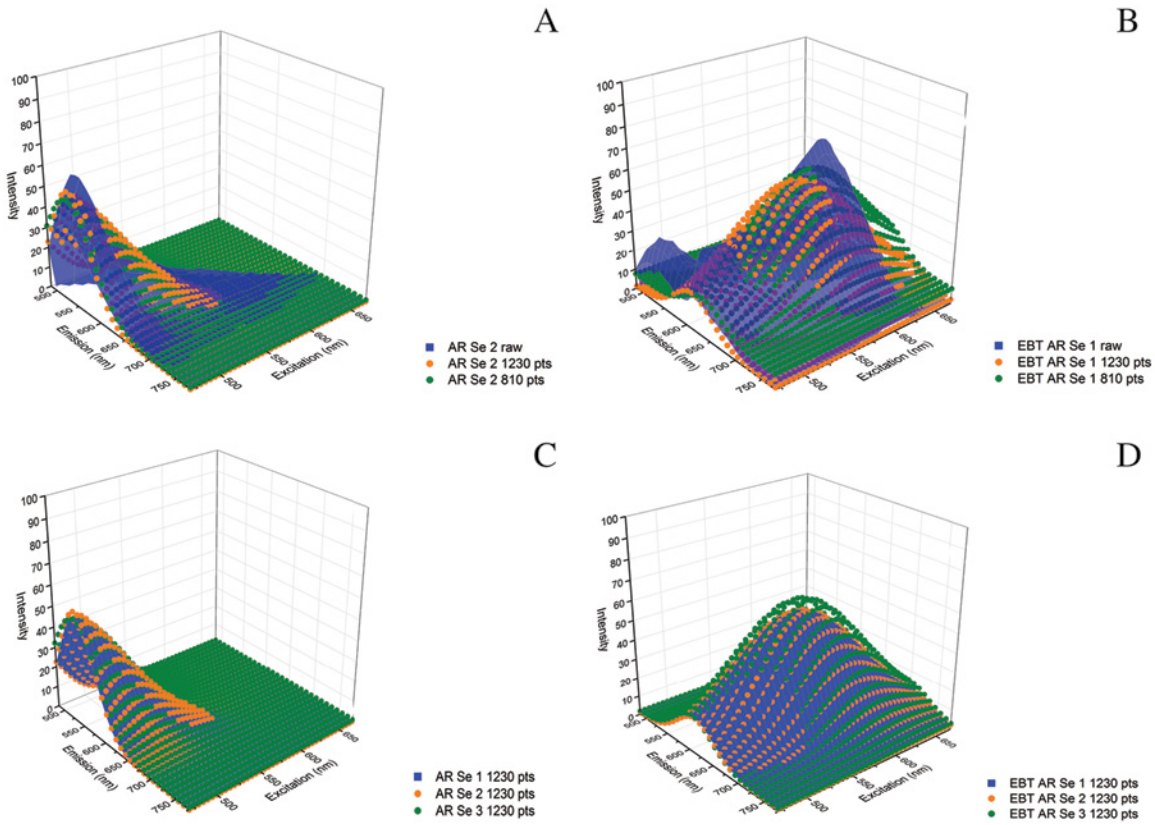

Figure 3. Functional fit of Λ^2 data to 2D Gaussian surfaces. Three-dimensional (3D) surface plots of raw Λ^2 data fit to the 2-dimensional (2D) Gaussian model: (A) Antigen retrieval (AR) and serum (Se) and (B) Eriochrome black T (EBT) AR Se. Data points: 1230 data points (pts) is the full raw data set; 810 pts is the next step in data point removal. The model fits generated from multiple data collections within a treatment align well: (C) AR Se models representing all three fields and (D) likewise for EBT AR Se. Filled and dot matrix surfaces are used solely for better visualization and have no additional meaning here or in later use in figures.

but no shift in those treated with EBT with no AR (Fig. 7C, 7D). Additionally, this right shift was an obvious shift from baseline for the EBT AR treatments; e.g., AR No Se vs. EBT No AR No Se vs. EBT AR No Se at both excitations (Fig. 7E, 7F).

Sodium Borohydride Dampens Autofluorescence Universally

As demonstrated in representative 3D surface plots, NB markedly dampened autofluorescence across the spectra, regardless of the presence of AR and Se (Fig. 8A). Moreover, AR and Se applications appeared to enhance this effect (Fig. 4C and Supplemental Fig. 6); however, this finding was not significant (Table 3). Although, the central peak of intensity did not move, grouping with AR Se (Fig. 8B), the change in mean intensity following NB treatment was significant, along with SB AR Se (see below) (Fig. 4C). These treatments grouped statistically separately from AR Se and there was no significant difference in the two NB treatments' groupings (Table 3). The line graphs of 458 nm and 405 nm excitation emissions also revealed decreases in autofluorescence (Fig. 8C, 8D) and the intensity averages for both NB treatments grouped together (Tables 4, 5).

Sudan Black B Quenches Autofluorescence, and Combined Treatments Yield Mixed Results

SB AR Se had a similar result as NB, with a greater magnitude of autofluorescence intensity change (Fig. 8E, 8B, and 4C). However, there was no significant difference between SB AR Se and the two NB treatments (Table 3). Similar changes to those above for NB were also seen with 458 nm and 405 nm excitations (Fig. 5C, 5D), where SB clearly lowered autofluorescence intensity more than that seen for any of the single treatments; yet it still grouped statistically with the two single NB treatments (Tables 4, 5). Finally, the excitation of the SB-treated

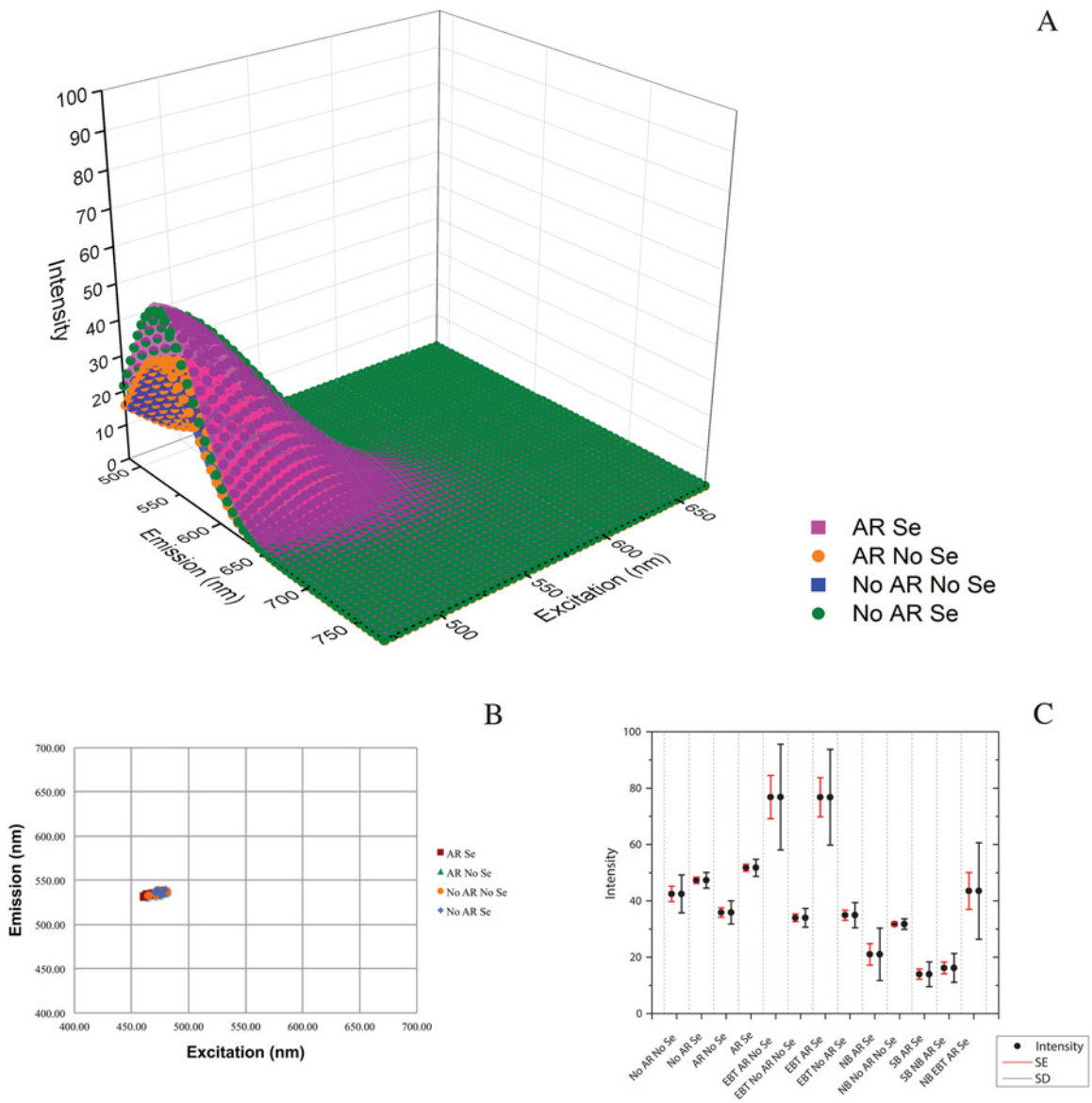

Figure 4. Antigen retrieval (AR) and serum (Se) application do not increase autofluorescence in formalin-fixed, paraffin-embedded human tracheal tissue in the 470–670 nm excitation range. A comparison of models and model outputs for AR Se, No AR No Se, AR No Se and No AR Se shows little difference in the four treatments. (A) Representative model fits. (B) A scatter plot of model variables x_c,y_c reveals that, for all model fits for all four baseline treatments, the central peak location of emission intensity is similar. (C) A box plot of all means of maximum intensity (sum A and z0) for all treatments collected by white light laser excitation 470–670 nm reveals a complete overlap for the four baseline treatments. Bars are SE (red) and SD (black). Intensity is a unitless, laser-dependent value.

slide with an MP laser resulted in boiling of the SB during excitation, an effect not observed with the EBT- or the NB-treated slides.

Combining SB and NB was no better than either treatment alone while combining EBT and NB appeared to result in further dampening of autofluorescence compared with these treatments alone, albeit, this latter finding was not statistically significant, as NB EBT AR Se grouped consistently with NB AR Se (Tables 3-5).

Treatments Tried on Frozen Liver Show Similar Results, and Mouse and Human Lung Have Similar Autofluorescence Profiles

Difficulty visualizing a FITC-conjugated antibody in frozen cirrhotic human liver tissue led to an opportunity to compare the autofluorescence diminishing capability of EBT and SB in a different human tissue type. As in human lung tissue, EBT application shifted the autofluorescence signal

Table 3. ANOVA Connected Letters Report for White Light Laser Excitation.

Treatment	Grouping					
AR Se		B				
No AR Se		B	C			
No AR No Se		B	C			
AR No Se		B	C	D		
EBT AR No Se	A					
EBT AR Se	A					
EBT No AR Se		B	C	D	E	
EBT No AR No Se		B	C	D	E	
NB AR Se				D	E	F
NB No AR No Se			C	D	E	F
SB AR Se					E	F
NB SB AR Se						F
NB EBT AR Se		B	C	D		
AR Se		B				
EBT AR Se	A					
NB AR Se				D	E	F
SB AR Se					E	F
NB SB AR Se						F
NB EBT AR Se		B	C	D		

These ANOVA results support the data shown in Fig. 4C. Treatments not sharing a letter (grouping) are significantly different from each other ($p<0.05$). Treatments sharing a letter are not. Abbreviations: AR, antigen retrieval; Se, serum; EBT, Eriochrome black T; NB, Sodium borohydride; SB, Sudan black B.

to the right whereas SB lowered the intensity of the autofluorescence signal without shifting the central peak of emission (Supplemental Fig. S7). Additionally, we found mouse lung tissue fixed in 10% neutral-buffered formalin had a similar autofluorescence signature to that seen in equivalently fixed human lung tissue as did mouse lung fixed in the alternative fixative HistoChoice (data not shown).

Discussion

This study was designed to evaluate methods to decrease tissue autofluorescence in FFPE respiratory tissue sections in order to more successfully visualize fluorescent markers of interest. Steam AR in a pH 6 citrate buffer and serum application—both common steps in immunofluorescence protocols—did not increase autofluorescence. A number of treatments to decrease tissue autofluorescence were evaluated, and we found that EBT, SB, and NB were the most effective at diminishing tissue autofluorescence. In order to more quantitatively study the efficacy of these treatments, mathematical modeling of changes in autofluorescence was performed and shown to be an effective technique for the analysis of treatment efficacy.

The treatments we did not carry forward into further analysis were not all ineffective on respiratory tissues, and those that were ineffective, might be effective when used on other tissue types with different endogenously autofluorescent elements. For example, lipofuscin, an autofluorescent red blood cell breakdown product found in hepatocytes, is not present in respiratory tissue (Schnell et al. 1999). Additionally, our use of light irradiation to diminish autofluorescence was restricted to a narrow UVB band (280–320 nm) quite distant from the peak excitations we measured in the 400-nm range. The broader band irradiation of tissue presented by Neumann and Gabel (2002), although attractive and likely quite efficacious, was not feasible due to facility limitations.

As captured using Λ^2 analysis on the Leica SP5 WLL confocal system, human tracheal tissue that is fixed in neutral-buffered formalin and then embedded in paraffin has an autofluorescence profile that fits a 2D Gaussian surface with a central peak of intensity with an excitation in the 470s nm, and emission in the 530s nm (No AR No Se tissue). This aligns the peak autofluorescence well with the emission of FITC, thereby explaining the difficulty with FITC immunofluorescence on this tissue type, a commonly reported finding (Baschong et al. 2001; Beisker et al. 1987; Callis 2006; Clancy and Cauller 1998; Cowen et al. 1985; Kittelberger et al. 1989; Neumann and Gabel 2002; Schenk and Churukian 1974).

In this study, neither steam AR with a pH 6 citrate buffer nor application of 5% donkey serum increased autofluorescence significantly. We did not explore steam AR with EDTA or alternative pH citrate buffers. Additionally, we did not explore microwave-, enzymatic- or pressure cooker-based AR. We suspect that the latter would be the same, as we have found anecdotal evidence that both pressure cooker- and vegetable steamer-based AR are quite comparable in their effects on tissue samples. Also, we did not explore other blocking reagents; therefore, there is the possibility that other blocking reagents might increase autofluorescence. Moreover, if excess quantities of these blocking reagents are not removed in subsequent washes, their residues might also increase autofluorescence.

EBT is easy to apply and consistent in shifting autofluorescence from the green to red wavelength emission range when applied to steam AR-treated tissues. We are uncertain of the basis for this observation, but EBT as a complex-sensitive indicator can complex with Ca^{++} and other divalent metals thereby changing from blue to red (Dubenskaya and Levitskaya 1999). Additionally, EBT has a polar group and therefore would be expected to have its effects in the water-soluble portion of the sample. The shift from the green to red wavelength resembles an excitation energy transfer from the autofluorescent species to a new chromophore—the bound EBT perhaps. If so, then EBT or modified EBT absorbs the autofluorescence emission, thereby reducing its intensity, then emits at the higher wavelength. The divalent metal-complexed red form, which absorbs at a

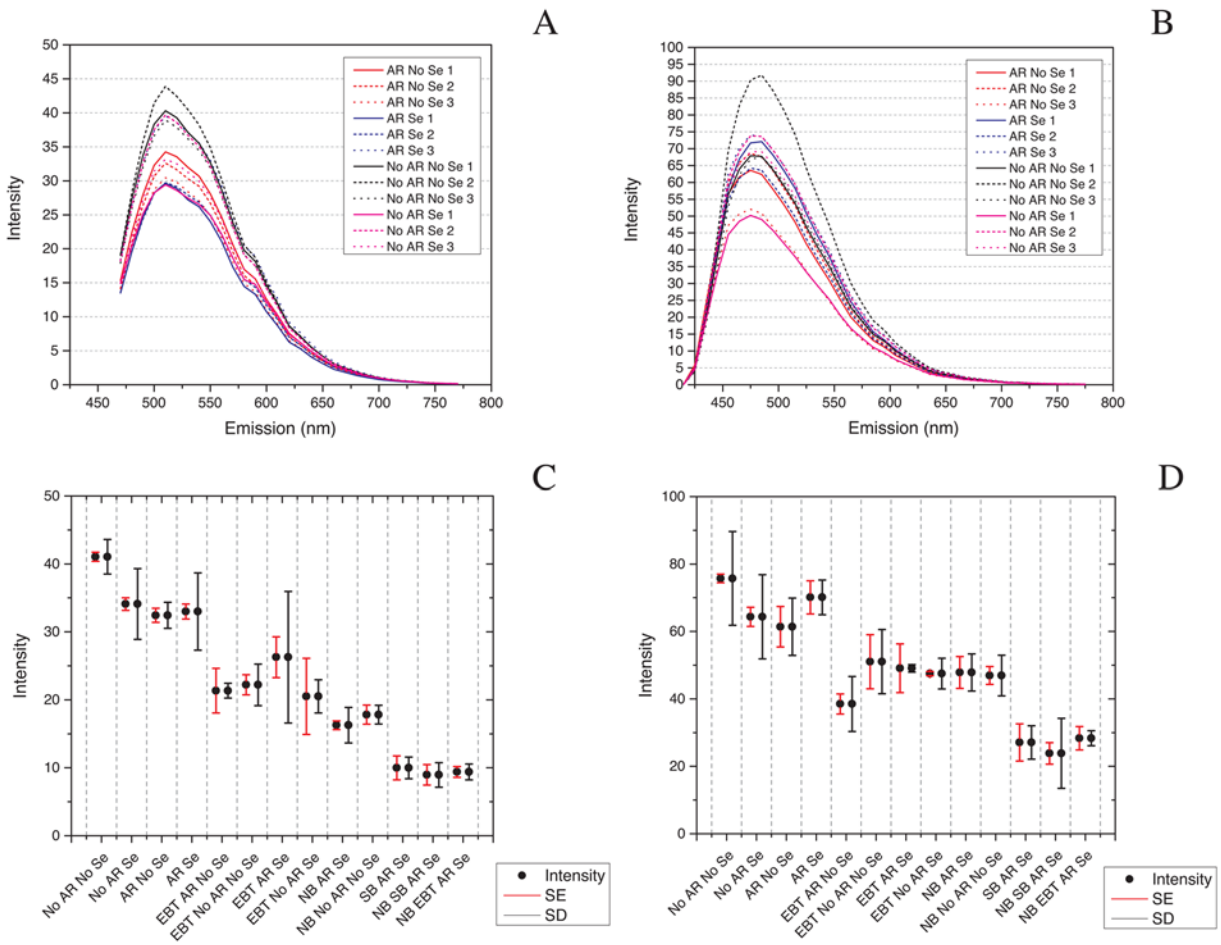

Figure 5. Antigen retrieval (AR) and serum (Se) application do not increase autofluorescence in formalin-fixed, paraffin-embedded human tracheal tissue at 458 nm or 405 nm excitations. Emission line graphs for the four baseline treatments (AR Se, No AR No Se, No AR Se, and AR No Se) at 458 nm excitation (A) and 405 nm excitation (B); box plots of the means of maximum intensity (sum A and z0) for all treatments at 458 nm excitation (C); and 405 nm excitation (D) reveal little variance at 458 nm and 405 nm excitations for the four baseline treatments. Bars on box plots are SE (red) and SD (black). Intensity is a unitless, laser-dependent value.

lower wavelength than the blue form, is more likely to be the absorbing species (Dubenskaya and Levitskaya 1999). AR may expose epitopes for EBT binding, thereby producing a new fluorescent species. Alternatively, EBT may form this species by reacting with a residual component from the AR step. At times we noticed that the green to red wavelength shift was incomplete, which presented as a small second peak in the WLL data (Fig. 3B). Additionally, dual peaks were present consistently on the 458 nm and 405 nm emission graphs (Fig. 7A and 7B). Therefore, increased EBT concentrations may diminish green wavelength autofluorescence even further.

Based on the model outputs, the post-treatment intensity for EBT AR with or without Se was significantly stronger than the original peak autofluorescence in the green wavelengths. Although this may be true, it is more likely that the intensity in the red wavelengths is the same as or less than that seen prior to treatment in the green wavelengths due to an innate characteristic of the WLL system. Power output of the WLL, particularly at the 60% level used to enable good mathematical model fits across all treatments in this project, varied by wavelength (Supplemental Fig. S1). Therefore, a comparison of treatments that diminish autofluorescence without shifting the central peak of this autofluorescence is straightforward. However, comparing treatments that shift autofluorescence to those that do not or those that shift it differently is difficult. We did not undertake the additional data collection needed to examine the entire profile of WLL power variation. Additionally, it is unclear how these data might be used to normalize intensity. So, although we are confident that the EBT shifted the autofluorescence peak to the right, we are uncertain whether the peak is more,

Table 4. ANOVA Connected Letters Report for 458 nm Excitation.

Treatment	Grouping							
AR Se	A	B	C					
No AR Se	A	B						
No AR No Se	A							
AR No Se	A	B	C	D				
EBT AR No Se				D	E	F		
EBT AR Se		B	C	D	E			
EBT No AR Se					E	F	G	
EBT No AR No Se			C	D	E			
NB AR Se					E	F	G	H
NB No AR No Se					E	F	G	H
SB AR Se						F	G	H
NB SB AR Se								H
NB EBT AR Se							G	H
AR Se	A	B	C					
EBT AR Se		B	C	D	E			
NB AR Se					E	F	G	H
SB AR Se						F	G	H
NB SB AR Se								H
NB EBT AR Se							G	H

These ANOVA results support the data shown in Fig. 5C. Treatments not sharing a letter (grouping) are significantly different from each other ($p<0.05$); treatments sharing a letter are not. Abbreviations: AR, antigen retrieval; Se, serum; EBT, Eriochrome black T; NB, sodium borohydride; SB, Sudan black B.

Table 5. ANOVA Connected Letters Report for 405 nm Excitation.

Treatment	Groupings					
AR Se	A	B				
No AR Se	A	B				
No AR No Se	A					
AR No Se	A	B	C			
EBT AR No Se			C	D	E	F
EBT AR Se		B	C	D	E	
EBT No AR Se		B	C	D	E	F
EBT No AR No Se		B	C	D		
NB AR Se		B	C	D	E	
NB No AR No Se		B	C	D	E	F
SB AR Se					E	F
NB SB AR Se						F
NB EBT AR Se				D	E	F
AR Se	A	B				
EBT AR Se		B	C	D	E	
NB AR Se		B	C	D	E	
SB AR Se					E	F
NB SB AR Se						F
NB EBT AR Se				D	E	F

These ANOVA results support the data shown in Fig. 5D. Treatments not sharing a letter (grouping) are significantly different from each other ($p<0.05$); treatments sharing a letter are not. Abbreviations: AR, antigen retrieval; Se, serum; EBT, Eriochrome black T; NB, sodium borohydride; SB, Sudan black B.

equivalently, or less intense, as the WLL power applied to the tissue increases as one moves from the high 400s nm excitation to the mid-500s nm (Supplemental Fig. S1). Consequently, this implies that the significant ANOVA findings, where EBT AR Se and EBT AR No Se are grouped differently from all other treatments, must be interpreted cautiously.

We can, however, examine single windows of this intensity increase issue by examining the 458 nm and 405 nm excitation intensity data. At both 458 and 405 nm excitations, the EBT treatments did not group separately from the four AR, Se combinations, indicating that this intensity in the red wavelengths for EBT AR Se and EBT AR No Se is likely equivalent in intensity to the green wavelength autofluorescence seen for the four AR, Se combinations and the EBTs that did not receive AR. Thus, we recommend EBT as a treatment for autofluorescence in combination with AR so long as one does not plan to use a marker that emits in the red wavelengths.

NB diminished autofluorescence without changing the location of the central peak of its emission. Its primary mechanism of action for diminishing autofluorescence is via a reduction in the introduction of aldehydes and amine-aldehydes from formalin fixation to the respective alcohols (Baschong et al. 2001; Clancy and Cauller 1998). We recommend NB as a treatment for diminishing autofluorescence. However, its use is a bit more involved than EBT, requiring a chemical hood and attended incubations. If left on for too long or in too high concentration, the tissue may detach from the slides.

The effect of SB on tissue autofluorescence mimicked that of NB. As with EBT, we are not certain of its mechanism of action. Unlike EBT, SB is lipid soluble. It absorbs at 580 nm (Thakur et al. 1989) so may absorb a small amount of tissue autofluorescence. Additionally, its quenching action may be attributable to absorption of autofluorescence, direct chemical interactions with autofluorescent species, or other causes. Preparation and application of SB is, again, more involved than that of EBT. In particular, the post-incubation removal of the reagent is a fine dance between leaving residual black particulate matter adhered to the slide and removing all dye and, consequently, its autofluorescence-diminishing effect. Additionally, we observed boiling of residual SB when the tissue was excited by a multi-photon laser.

In summary, we show that bright-field microscopy image clarity varied between the three treatments: NB, EBT and SB. We did not discern a difference between AR Se- and NB AR Se-treated tissues under the bright-field

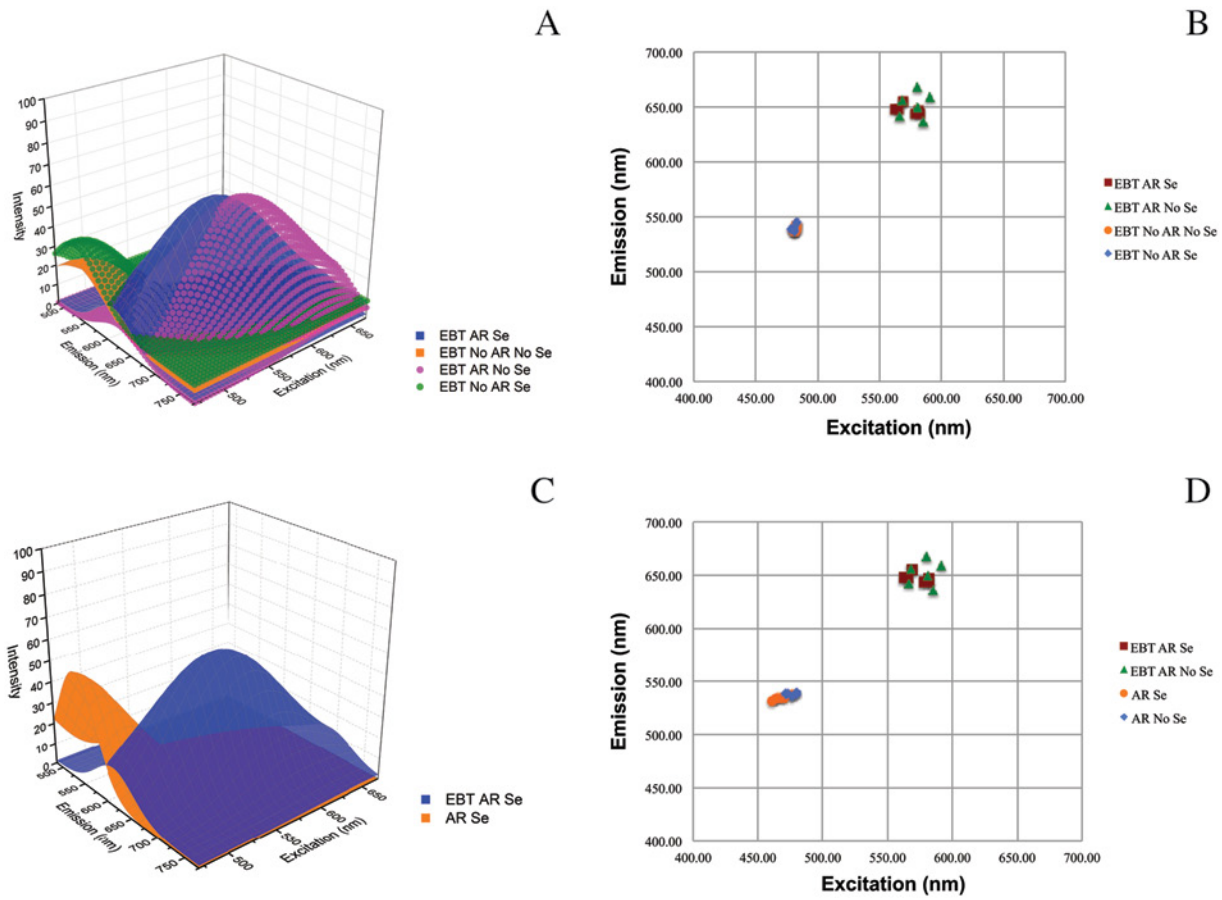

Figure 6. Eriochrome black T (EBT) with antigen retrieval (AR) shifts formalin-fixed, paraffin-embedded human tracheal tissue autofluorescence to the right. AR is required to achieve an effect with EBT. (A) 3D surface plots of representative models of the four treatments (EBT AR with Serum (Se), EBT AR without serum (No Se), EBT No AR No Se, EBT No AR Se). (B) Scatter plot of central peaks of emission for all EBT model fits. (C) 3D surface plots of model for EBT AR Se vs. AR Se. (D) Central peak of emission scatter plot for AR treatments with and without EBT.

microscope. EBT AR Se-treated tissue elements were lightly outlined in black whereas SB AR Se-treated tissues were not only outlined in darker black stain but also had residue that frequently blocked the visibility of tissue elements even after thorough wash steps. We found no significant additional diminishment of autofluorescence when using SB or EBT in combination with NB. Consequently, neither approach was considered to be efficacious in this study. However, on another tissue type, or even on respiratory tissue with additional optimization of the concentrations or incubation steps, a combination treatment might yield an improvement over the treatment with the single reagent.

These findings can be extrapolated to FFPE human respiratory tissues in general based on our observations during the 9-treatment comparison wherein treatment effects on lung mirrored those on trachea. We also saw that the untreated tissue autofluorescence signature of mouse lung mimicked that seen in human respiratory tissues, irrespective of whether the tissue was fixed in neutral-buffered formalin or HistoChoice. Likely, the autofluorescence treatment responses in the wider mouse respiratory tract would be similar to those that we saw in human trachea. The application of the mathematical modeling technique presented here would enable validation of this hypothesis. Finally, elements of this study provide a starting point for improving our understanding of autofluorescence in other tissue types regardless of their preparation. The autofluorescence profile of frozen human liver was similar to that of human trachea; the application of EBT and SB also yielded similar results.

The technology and methodologies employed in this study have broader applicability. We regularly use Λ^2 analysis to ascertain marker(s) visibility above background

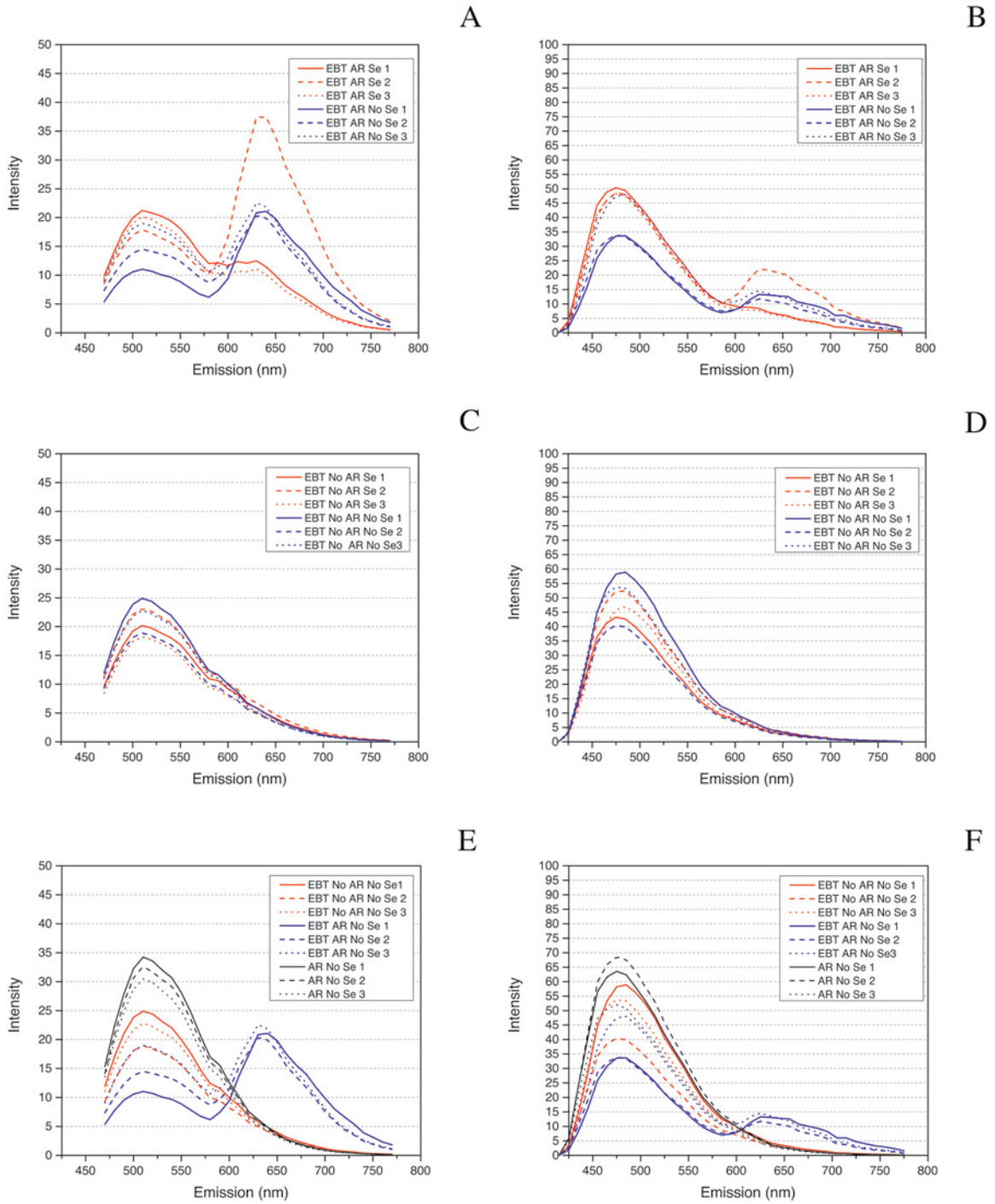

Figure 7. Impact of antigen retrieval (AR) with Eriochrome black T (EBT) is visible with 458 nm and 405 nm excitations. (A-B) Emission profiles for EBT and AR at 458 nm and 405 nm excitations, respectively. There is a partial shift in autofluorescence observed for EBT and AR-treated slides at 458 nm and 405 nm excitations. (C-D) Emission profiles for EBT and No AR at 458 nm and 405 nm excitation respectively. There is no shift observed with EBT treatment with AR is absent. (E-F) The EBT AR No Se emission profiles group separately from the EBT No AR Se and No AR Se profiles at the 458 nm and 405 nm excitation readings. This is seen as a partial right shift of the central peak of emission, visible as a double-peaked structure more prominently at 458 nm excitation than at 405 nm excitation.

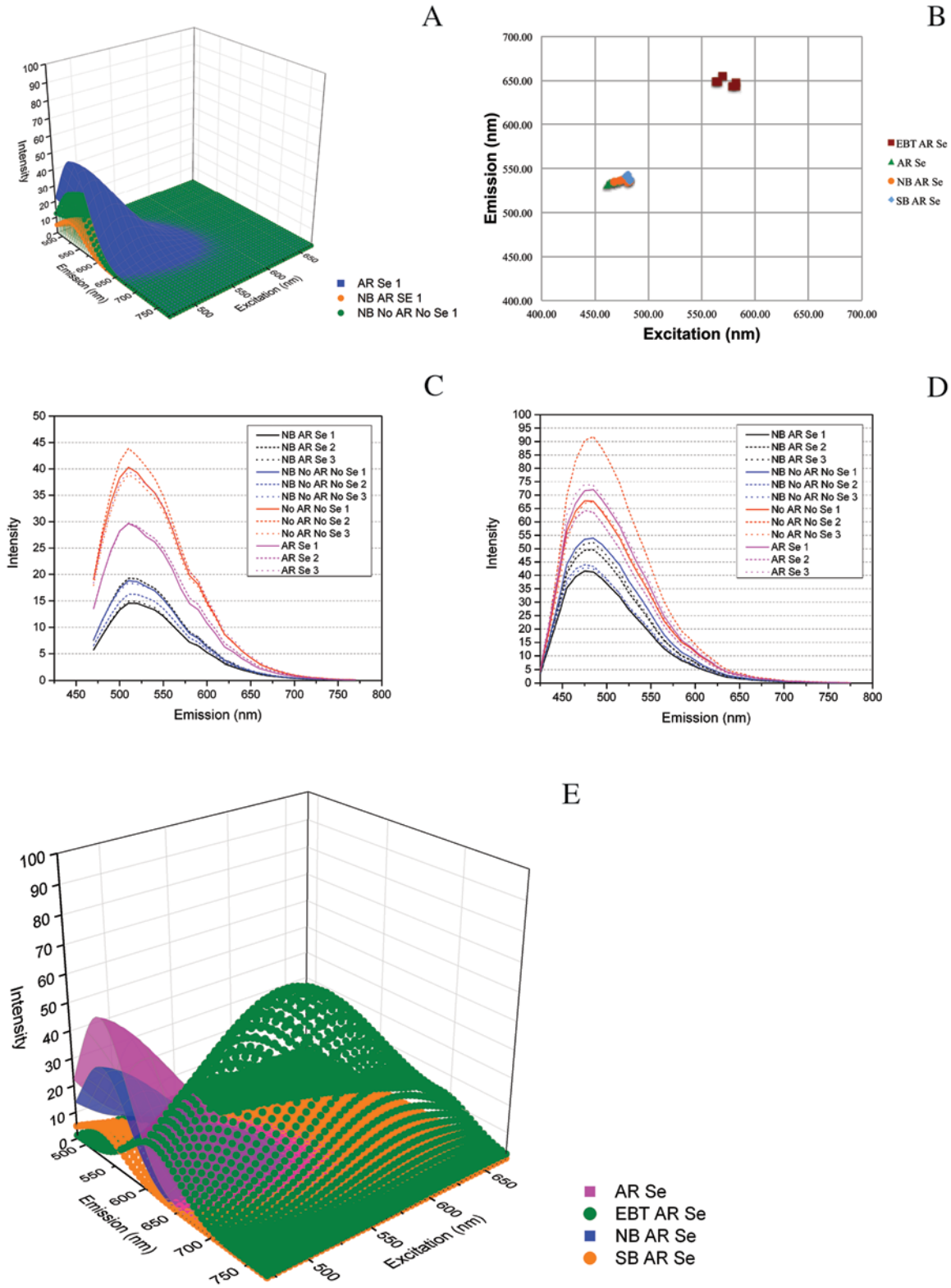

Figure 8. Sodium borohydride (NB) and Sudan black B (SB) are very effective quenchers of autofluorescence. Regardless of presence of antigen retrieval (AR) in the protocol, NB markedly quenched autofluorescence. (A) Comparison of models of NB with or without AR and serum (Se) to AR Se. (B) Central peaks of emission scatter plot showing there is no shift in the center of the tissue autofluorescence. This quenching of autofluorescence is also present at 458 nm and 405 nm excitations, respectively (C-D). A comparison of AR Se-based treatments alone (E) shows representative diminishment of autofluorescence by each treatment (AR Se, EBT AR Se, NB AR Se and SB AR Se).

autofluorescence with and without additional tissue treatments to diminish autofluorescence. These techniques might also be extended to analyses of shifts in a tissue's autofluorescence signature due to disease processes wherein an autofluorescent tissue component's organization and distribution is modified. Such work would first require better separation of the individual endogenous contributors to the tissue autofluorescence and the ability to identify them separately within the model. Such are the goals of the numerous studies focused on tissue fluorescence spectroscopy as well as techniques such as those reviewed in Cicchi et al. (2013) for collagen and elastin (Cicchi et al. 2013; Monici 2005).

In this study, we assessed several treatments for diminishing autofluorescence. Throughout, we used novel quantitative techniques that, to the authors' knowledge, have not been previously reported in the literature, including the development of a mathematical model for demonstrating the changes in autofluorescence. These techniques should prove broadly useful for investigating similar questions in different species, tissue types and even tissue preparations, as shown by our experimentation with FFPE mouse lung and frozen human liver tissues. In conclusion, we found EBT, NB and SB to be differently efficacious in diminishing autofluorescence in FFPE human respiratory tissue.

Acknowledgments

We thank Sandra Horton and her staff at the North Carolina State University College of Veterinary Medicine Histopathology Laboratory for their preparation of tissue sections for immunohistochemistry and autofluorescence treatments; Robert Cunningham, formerly at the Armed Forces Institutes of Pathology, for his autofluorescence treatment suggestions and support; Marta Melis at the Hepatic Pathogenesis Section, Laboratory of Infectious Diseases, NIAID for frozen liver tissue samples treated with Eriochrome black T and Sudan black B; Joe Kovacs and Geetha Kutty at the Critical Care Medicine Department, Clinical Center, NIH for providing HistoChoice-fixed paraffin-embedded mouse lung tissue slides; Alice Haddy, Professor Biophysical Chemistry, University of North Carolina Greensboro, for her insights into the mechanisms of action for EBT and SB; Katherine Davis for figure panel compilation assistance; and Owen Schwartz and Lily Koo of the NIAID Research Technology Branch Bioimaging Section for their technical assistance with the diverse types of microscopy employed in this study. ASD and JKT are further thankful for the support of the NIH Comparative Molecular Pathology Research Training Program. This work was completed in partial fulfillment of A. Sally Davis' dissertation work towards a PhD in Comparative Biomedical Sciences at North Carolina State University College of Veterinary Medicine.

Declaration of Conflicting Interests

The authors declared no potential conflicts of interest with respect to the research, authorship, and/or publication of this article.

Funding

The authors disclosed receipt of the following financial support for the research, authorship, and/or publication of this article: This research was supported by the intramural research funds of the NIH and the NIAID.

References

Banerjee B, Miedema BE, Chandrasekhar HR (1999). Role of basement membrane collagen and elastin in the autofluorescence spectra of the colon. J Investig Med 47:326-332.

Baschong W, Suetterlin R, Laeng RH (2001). Control of autofluorescence of archival formaldehyde-fixed, paraffin-embedded tissue in confocal laser scanning microscopy (CLSM). J Histochem Cytochem 49:1565-1572.

Beisker W, Dolbeare F, Gray JW (1987). An improved immunocytochemical procedure for high-sensitivity detection of incorporated bromodeoxyuridine. Cytometry 8:235-239.

Billinton N, Knight AW (2001). Seeing the wood through the trees: a review of techniques for distinguishing green fluorescent protein from endogenous autofluorescence. Anal Biochem 291:175-197.

Callis G (2006) Autofluorescence blocking [Online}. Available: http://www.uhnresearch.ca/facilities/wcif/PDF/Autofluorescence.pdf

Cicchi R, Vogler N, Kapsokalyvas D, Dietzek B, Popp J, Pavone FS (2013). From molecular structure to tissue architecture: collagen organization probed by SHG microscopy. J Biophotonics 6:129-142.

Clancy B, Cauller LJ (1998). Reduction of background autofluorescence in brain sections following immersion in sodium borohydride. J Neurosci Methods 83:97-102.

Collins TJ (Posted Online 04/04/2006). Autofluorescence: Causes and cures. Wright Cell Imaging Facility. Toronto Western Research Institute, University Health Network. Available: http://www.uhnresearch.ca/facilities/wcif/PDF/Autofluorescence.pdf.

Cowen T, Haven AJ, Burnstock G (1985). Pontamine sky blue: a counterstain for background autofluorescence in fluorescence and immunofluorescence histochemistry. Histochemistry 82:205-208.

Del Castillo P, Llorente AR, Stockert JC (1989). Influence of fixation, exciting light and section thickness on the primary fluorescence of samples for microfluorometric analysis. Basic Appl Histochem 33:251-257.

Dubenskaya LO, Levitskaya GD (1999). Use of Eriochrome black T for the polarographic determination of rare-earth metals. J Anal Chem 54:655-657.

Kittelberger R, Davis PF, Stehbens WE (1989). An improved immunofluorescence technique for the histological examination of blood vessel tissue. Acta Histochem 86:137-142.

Leica Microsystems (2010). Sp5x user interface: Lambda^2-mapping guideline [Online]. Available: http://www.leica-microsystems.com/fileadmin/downloads/LeicaTCSSP5X/UserManuals/SP5X_lambda_lambda_guideline.pdf.

Martinez-Anton A, Sokolowska M, Kern S, Davis AS, Alsaaty S, Taubenberger JK, Sun J, Cai R, Danner RL, Eberlein M,

Logun C, Shelhamer JH (2013). Changes in microRNA and mRNA expression with differentiation of human bronchial epithelial cells. Am J Respir Cell Mol Biol 49:384-395.

Monici M (2005). Cell and tissue autofluorescence research and diagnostic applications. Biotechnol Annu Rev 11:227-256.

Neumann M, Gabel D (2002). Simple method for reduction of autofluorescence in fluorescence microscopy. J Histochem Cytochem 50:437-439.

Schenk EA, Churukian CJ (1974). Immunofluorescence counterstains. J Histochem Cytochem 22:962-966.

Schnell SA, Staines WA, Wessendorf MW (1999). Reduction of lipofuscin-like autofluorescence in fluorescently labeled tissue. J Histochem Cytochem 47:719-730.

Thakur MS, Prapulla SG, Karanth NG (1989). Estimation of intracellular lipids by the measurement of absorbance of yeast cells stained with Sudan Black B. Enzyme Microb Technol 11:252-254.

Viegas MS, Martins TC, Seco F, do Carmo A (2007). An improved and cost-effective methodology for the reduction of autofluorescence in direct immunofluorescence studies on formalin-fixed paraffin-embedded tissues. Eur J Histochem 51:59-66.